Engineering Fracture Mechanics 78 (2011) 695–712

Contents lists available at ScienceDirect

Engineering Fracture Mechanics

journal homepage: www.elsevier.com/locate/engfracmech

Damage detection with genetic algorithms taking into account a crack contact model

Fernando S. Buezas [a,b,*], Marta B. Rosales [c,b], Carlos P. Filipich [c,d]

[a] Department of Physics, Universidad Nacional del Sur, 8000, Bahía Blanca, Argentina
[b] CONICET, Argentina
[c] Department of Engineering, Universidad Nacional del Sur Alem 1253, 8000 Bahía Blanca, Argentina
[d] CIMTA – Centro de Investigaciones en Mecánica Teórica y Aplicada, FRBB, Universidad Tecnológica Nacional, 11 de Abril 465, 8000 Bahía Blanca, Argentina

ARTICLE INFO

Article history:
Received 12 March 2010
Received in revised form 9 November 2010
Accepted 12 November 2010
Available online 19 November 2010

Keywords:
Crack detection
Genetic algorithm
Contact problem
Non-linear dynamics

ABSTRACT

This paper deals with the crack detection in structural elements by means of a genetic algorithm optimization method. The crack model takes into account the existence of contact between the interfaces of the crack. Many of the methods to detect a crack in beam-like structures are based on linear one dimensional models and are not straightforwardly applicable to structures such as beams or arcs with a breathing crack with or without contact. The present study addresses bi- and three-dimensional models to handle the dynamics of a structural element with a transverse breathing crack. The methodology is not restricted to beam-like structures since it can be applied to any arbitrary shaped 3D element. The crack is simulated as a notch or a wedge with a unilateral Signorini contact model. The contact can be partial or total. All the simulations are carried out using the general purpose partial differential solver FlexPDE, a finite element (FE) code. A genetic algorithm (GA) optimization method is successfully employed for the crack detection. The dynamic response at some points of the damaged structures are compared with the solution of the computational (FE) model using least squares for each proposed crack depth and location. An objective function arises which is then optimized to obtain an estimate of both parameters. Physical experiments were performed with a cantilever damaged beam and the resulting data used as input in the detection algorithm.

1. Introduction

In the review by Doebling et al. [6], Lifshitz and Rotem (1969) are mentioned as the authors of the first published article using the vibration data to diagnosis the damage. The computational resources and the experimental capacity to data acquisition were very limited at that time, which may explain that the first detection methods reported in literature are only based on natural frequency changes. From the obtained data, parameters related with the value of the stress tensor were found as indicators of the damage. Back to the 1980s finite elements started to be used as a computational tool to model damaged structural elements. Changes in the natural frequencies was the first and more studied criterion [20,5,16,12], and the detection of many cracks with this technique was reported in [5,16,10,12] . Some attempts to detect the damage from the inverse problem were included in studies [14,17]. Anyway, the bad conditioning makes the detection difficult to be tackled as a pure inverse problem. On the other hand, many works dealing with straight beams have been reported [6]. Wang and He [22] used artificial neural networks (ANN) to detect crack in arch structural elements. The authors of

* Corresponding author at: Department of Physics, Universidad Nacional del Sur, Av.Alem 1253, 8000 Bahía Blanca, Argentina.
E-mail address: fbuezas@gmail.com (F.S. Buezas).

0013-7944/$ - see front matter © 2010 Elsevier Ltd. All rights reserved.
doi:10.1016/j.engfracmech.2010.11.008

the present work have employed ANN in beam-like structures and rotating beams [19]. Genetic algorithms appear as an attractive approach [8] to optimize an objective function that depends on the crack position and magnitude when a nonlinear dynamic is present, either due to large rotations or contact at the crack closing. Research in this direction can be found in [3,1,4,18]. On the other hand, contact at the crack can be modeled in many ways. Carneiro [2] proposed a breathing crack model for a Timoshenko beam. Contact models have been employed in other areas of the Mechanics by Raous [18] and Kikuchi and Oden [11]. A thorough and detailed study of the mechanics of contact can be found in [9]. The structural models implemented in the present work are referred to the undeformed configuration or Lagrangian description using the first and second Piola–Kirchoff tensors [13,7,21].

The present study deals with bi- and three-dimensional models to handle the dynamics of a structural element with a transverse breathing crack. The methodology is not only restricted to beam-like structures but it can be also applied to any arbitrary shaped 3D element. The crack is simulated as a notch or a wedge with a unilateral Signorini contact model. The contact may be partial or total. All the simulations are carried out using the finite element code FlexPDE, a general purpose, partial differential equation solver.

A genetic algorithm (GA) optimization method is successfully employed for the crack detection. The dynamic response at some points of the damaged structures are compared with the solution of the computational (FE) model using least squares for each proposed crack depth and location. An objective function arises which is then optimized to obtain an estimate of both parameters. The optimization algorithm is developed within the MatLab environment and interacts with the FEM model. It was found that the functions exhibit a large number of local minima. Given such a complexity, the standard optimization techniques (e.g. gradient methods) are not successful when used directly. Alternatively, the GA used herein, shows very acceptable behavior. Extensive studies were carried out to analyze the influence of the various parameters involved in the GA. The parametric studies allowed to set the optimal values of GA variables for this problem like population, reproduction, number of generations, etc.

Several cases regarding crack detection in beam-like structures have been analyzed within the present study. Physical experiments were performed with a cantilever damaged beam and the resulting data used as input in the detection algorithm. A general isotropic linear constitutive relationship between the second Piola–Kirchoff stress tensor and the Green-St. Venant strain tensor was proposed. The advantage of a general model (nonlinear) is that not only finite deformations can be considered, but also the reformulation of the problem for a rotational motion is not necessary. Additionally and when dealing with numerical experiments, a white noise was introduced and it was found that the errors remained in the same range. As the procedure is not restricted to beam-like elements, other geometries were tackled, *e.g.* an arch (curved beam) and a blade-like structural element (in 3D domain) in rotational motion, justifying the general nonlinear model. The methodology allows up to a third level detection, *i.e.* detection of damage existence, location and depth. Despite the inherent complexity of the problem, the resulting errors remain within reasonable values.

2. Statement of the problem

The crack detection will be performed on structural elements that will be tackled with two and three dimensional finite element models. In what follows, a brief introduction on the governing equations within the Solid Mechanics field will be stated. Also, the contact issue at the crack interface will be described. The beam problem (Fig. 1) is the structural element more extensively studied since it allows for adjustments and validation but any arbitrary shaped structure (2D or 3D) could be handled.

2.1. Equations of motion

The statement of the governing equations is made within the frame of Continuum Mechanics with a Lagrangian or material reference. Following this approach, only the next equation should be solved,

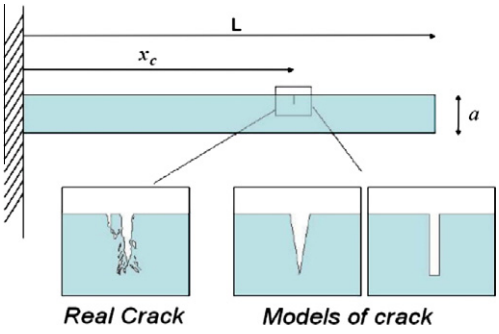

Fig. 1. Real crack and the detection model.

$$\nabla \cdot \mathbf{P} + \rho_0 \mathbf{b} = \rho_0 \mathbf{A} \tag{1}$$

where $\mathbf{P}$ is the first Piola–Kirchoff stress tensor [13,7,21] , $\rho_0 = \rho\ (\mathbf{X},\ t_0)$ is the initial density (which is known) and $\mathbf{A} = \partial \mathbf{V}/\partial\, t = \partial^2 \mathbf{x}/\partial t^2$, $\mathbf{x}$ is the position vector function of $\mathbf{X}$ (material coordinate), t is the time, and $\mathbf{A}$ is the acceleration field, that is simply the partial derivative of the velocity field $\mathbf{V}$.

The boundary conditions are imposed to the initial boundary (its position is known), leaving the statement of the boundary problem, the initial conditions and the equations of motion consistently closed. The boundary conditions are

$$\mathbf{x}(\partial V^1) = \bar{\mathbf{x}} \tag{2}$$

$$\mathbf{t}_0(\partial V^2) = \bar{\mathbf{t}}_0 \tag{3}$$

where $\mathbf{t}_0$ is the tension vector of Piola–Kirchhoff calculated for the expression $\mathbf{t}_0 = \mathbf{PN}$, $\mathbf{N}$ is the referential unit vector normal to the surface, ∂V^1 and ∂V^2 are parts of the contour in which geometric and natural boundary conditions correspond, respectively. Thus, the problem at the boundary, as well as the initial conditions and the equations of motion, are fully stated. The position of any point of the body, including the boundary, will be known once the differential problem is solved. The nonlinear part is transferred to the tensor $\mathbf{P}$. This tensor is non-symmetric. The second Piola–Kirchhoff tensor $\mathbf{S}$ is symmetric and given by $\mathbf{P} = \mathbf{FS}$, where $[\mathbf{F}]_{ij} = \partial x_i/\partial X_j$ is the deformation gradient tensor, x_i is the ith component of the displacement vector $u(\mathbf{X},\ t) = \mathbf{x}(\mathbf{X},\ t) - \mathbf{X}$, X_j is the jth component of the material vector field $\mathbf{X}$. Thus, the equations of motion are written as:

$$\nabla \cdot (\mathbf{FS}) + \rho_0 \mathbf{b} = \rho_0 \mathbf{A} \tag{4}$$

We need to relate $\mathbf{S}$ with the motion to complete the differential problem that has vector $\mathbf{u}$ (or $\mathbf{x}$) as an unknown. Both tensor, $\mathbf{P}$ and $\mathbf{S}$ are related to the Cauchy tensor $\boldsymbol{\sigma}$ through

$$\mathbf{FS} = (\det \mathbf{F})\boldsymbol{\sigma}(\mathbf{F}^{-1})^T = \mathbf{P} \tag{5}$$

Here the following constitutive equation is proposed:

$$\mathbf{S} = \lambda tr(\mathbf{E})\mathbf{I} + 2\mu\mathbf{E} + \mu_{int}\dot{\mathbf{E}} \tag{6}$$

where λ, μ and μ_{int} are constants, $\mathbf{E}$ is the Green's strain tensor

$$[\mathbf{E}]_{ij} = \frac{1}{2}\left(\frac{\partial u_i}{\partial X_j} + \frac{\partial u_j}{\partial X_i} + \frac{\partial u_k}{\partial X_i}\frac{\partial u_k}{\partial X_j}\right)$$

and $\dot{\mathbf{E}}$ is the material derivative of $\mathbf{E}$. Eq. (6) is known as St. Venant–Kirchhoff material model with internal viscous type dissipation [21] that, as is obvious, tends to Hooke's law for infinitesimal displacements, elastic homogenous and isotropic bodies (if $\mathbf{E} \to \boldsymbol{\varepsilon}$ and $\mu_{int} = 0$ then $\mathbf{S} \to \sigma = \lambda\ tr(\boldsymbol{\varepsilon})\mathbf{I} + 2\mu\boldsymbol{\varepsilon}$), λ and μ are the Lamé constants $\lambda = \nu E/(1+\nu)(1-2\nu)$, $\mu = E/2(1+\nu)$, ν is the Poisson's coefficient and E the modulus of elasticity, and $2\varepsilon_{ij} = \partial\, u_i/\partial x_j + \partial u_j/\partial x_i$ is the infinitesimal deformation tensor.

3. Contact models

In this section, a unilateral contact model between bodies undergoing arbitrary deformations is described. This type of problems presents large difficulties on the one hand due to the nonlinearities and on the other, due to the difficulty of stating and solving a non-holonomic restrictions problem, as the present one. The regularization to a holonomic problem makes it solvable and enables the study of more complex models that include friction, adhesion, etc.

3.1. Real contact surface

The contact surface between two rough bodies is partial. As the pressure increases, the borders irregularities deform thus increasing the contact area. Not only the mechanical issue but also chemical reactions, electrical and thermal effects are present in the contact, though not enough understood yet. In the present study, the authors do not consider the physical and chemical tribology issues.

3.2. Unilateral contact

As a first approach to the contact model let us suppose that a deformable body interacts with a rigid and fixed obstacle. The contact condition is the non-penetration of the body in the rigid obstacle.

3.2.1. Signorini problem

Let a body B with domain Ω be in the space (or in a plane). B has a sufficiently smooth boundary $\Gamma = \Gamma_F \cup \Gamma_D \cup \Gamma_C$ which is in contact with other body R that is rigid and fixed in the plane (see Fig. 2). Part Γ_F of the boundary Γ corresponds to the boundary where the stresses are prescribed (natural conditions of the problem) (Eq. (3)). Γ_D corresponds to the part of the boundary where the displacements are prescribed (geometric conditions) (Eq. (2)) and Γ_C is the part in contact with

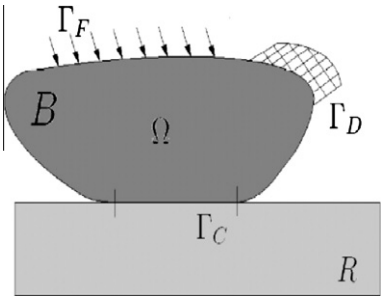

Fig. 2. Scheme of contact between a deformable body and a rigid obstacle.

the rigid body R. At the contact region Γ_C, the displacements $\mathbf{u}$ and stresses $\mathbf{t}_c$ may be decomposed in normal and tangential components in the following way

$$\mathbf{u} = u_N \mathbf{e}_n + u_T \mathbf{e}_t \tag{7}$$

$$\mathbf{t}_c = t_{cN} \mathbf{e}_n + t_{cT} \mathbf{e}_t \tag{8}$$

The Signorini problem (unilateral contact) is (see Fig. 3a)

$$\begin{cases} u_N \leqslant 0 \\ t_{cN} \leqslant 0 \\ u_N t_{cN} = 0 \end{cases} \tag{9}$$

It is easy observed that the Signorini conditions (9) are satisfied only with one of the following possibilities

1. No contact $\Rightarrow u_N \leqslant 0$ and $t_{cN} = 0$.
2. Contact $\Rightarrow u_N = 0$ and $t_{cN} \leqslant 0$.

The conditions (Eq. (9)) constitute a non-continuous or non-smooth problem since t_{cN} is a multi-valued application of the field u_N (or simply t_{cN} is not function of u_N). From the Analytical Mechanics viewpoint, the Signorini problems yields non-holonomic constraints given by inequalities. This is apparent in the fact that neither the stresses nor the contact surface itself are known before solving the problem. If this were solved, the deformation could be calculated but they are necessary to the statement of the classical boundary problem. In other words, within Continuum Mechanics, the knowledge of the boundary conditions is mandatory to solve the problem, but on other hand the Signorini problem deals with the boundary conditions as unknowns.

3.2.2. Extensions

Regarding the contact between two deformable bodies or two parts of the same body, the Signorini problem allows to easily solve the contact problem if the deformations and displacements are infinitesimal, by making a change of variable. Now, the problem is double: one for each body surface and, in the present study, one for each crack interface.

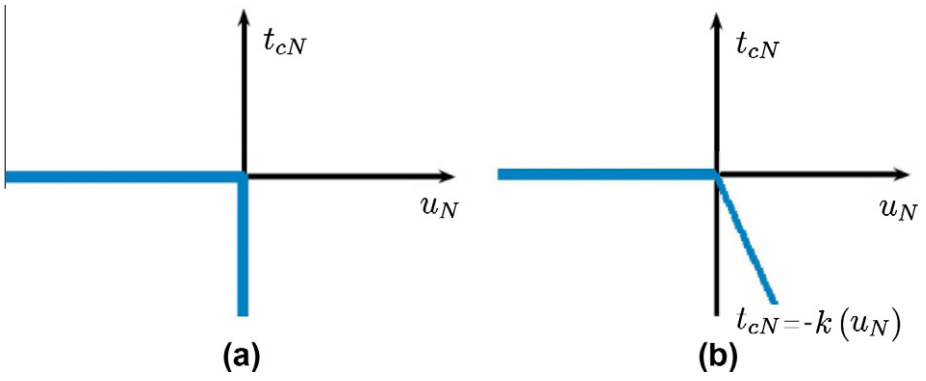

Fig. 3. (a) Signorini's law. t_{cN} is a multi-valued function of u_N at zero. (b) Regularization of Signorini's law. t_{cN} is continuous function of u_N at zero.

$$\text{body 1}\begin{cases} d(x_1,x_2) \geqslant 0 \\ t_{cN1} \leqslant 0 \\ x_1 t_{cN1} = 0 \end{cases} \quad \text{body 2}\begin{cases} d(x_2,x_1) \geqslant 0 \\ t_{cN2} \leqslant 0 \\ x_2 t_{cN2} = 0 \end{cases}$$

where $d(x_1, x_2)$ is the distance between the spacial points x_1 that belong to body 1 and x_2, to body 2. The advantage in using infinitesimal displacements is that unit vectors $N2 = -N1$ and the pair of points x_1 and x_2 are known before solving the problem and are on the surface normal.

Instead, if the displacements or deformations were finite, there would be no knowledge regarding which pair of point would be in contact nor the corresponding unit normal vectors. The smallest distance between all pair of points (one of each body) should be calculated and also unit normal vectors for such pair of points evaluated.

$$\text{body 1}\begin{cases} \min(d(x_1,x_2)) \geqslant 0 \\ t_{cN1} \leqslant 0 \\ x_1 t_{cN1} = 0 \end{cases} \quad \text{body 2}\begin{cases} \min(d(x_2,x_1)) \geqslant 0 \\ t_{cN2} \leqslant 0 \\ x_2 t_{cN2} = 0 \end{cases} \tag{10}$$

3.2.3. Regularization of the non-holonomic Signorini problem

The contact law stated in the previous subsection is of non-holonomic type, since no regular equation given by an equality exists. Instead, the contact problem poses a restriction given by a set of inequalities. The intermittency between a natural type condition and other of geometric type is what gives the non-regular character to the contact problem. The moment when the condition shifts from one to other state is an unknown of the problem.

The regularization idea consists in replacing the rigid condition by a smooth or regular one. The non-holonomic restriction problem is replaced by a non-constrained problem. The boundary condition will always be natural with the imposition of a functional relationship between stresses and displacements.

$$t_{cN} = \begin{cases} -k(v_N) & \text{if} \quad u_N > 0 \\ 0 & \text{else where} \quad u_N \leqslant 0 \end{cases} \tag{11}$$

where k is a number that, if sufficiently large, the problem given by Eq. (11) approximates to Eq. (9) (see Fig. 3b).

4. Computational simulations: equations of motion stated in the weak form and Galerkin's method

First let us write the weak formulation of the equations of motion. Let **W** be a test vector field (admissible functions) of variables referred to the body in its non deformed configuration (Lagrangian description). Multiplying the equations of motion by **W** and integrating over the body domain V, we get:

$$\int\int_{\partial V} (\mathbf{t}_0 \cdot \mathbf{W}) dA_0 + \int\int\int [\rho_0(\mathbf{b} - \mathbf{A}) \cdot \mathbf{W} - \mathbf{P} \cdot \nabla_X \mathbf{W}] dV = 0 \tag{12}$$

where (12) is obtained after integrating by parts (using the Green's formula).

The surface integral is divided in two parts. Suppose than the displacement **u**, and consequently the velocity **V**, is prescribed at a part of the boundary's surface (Γ_D in Fig. 2) and the stress is given at the other part (Γ_F). In order to incorporate the boundary conditions (2) and (3) in the weak form (12), first trial functions **W** (admissible test functions) are defined as

$$\mathbf{W}(\mathbf{X}) \in Adm_1 = \left\{ \mathbf{W} | \mathbf{W} = 0 \text{ on } \Gamma_D \quad \text{and} \quad \int (\nabla \mathbf{W})^2 dV < \infty \right\}$$

and the solution $\mathbf{u}(\mathbf{X},t)$

$$\mathbf{u}(\mathbf{X},t) \in Adm_2 = \left\{ \mathbf{u} | \mathbf{u} = \bar{\mathbf{x}} - X \text{ on } \Gamma_D \quad \text{and} \quad \int (\mathbf{P})^2 dV < \infty \right\}$$

Then the surface integral in Eq. (12) reduces to

$$\int\int_{\partial V} (\mathbf{t}_0 \cdot \mathbf{W}) dA = \int\int_{\Gamma_F} (\mathbf{t}_0 \cdot \mathbf{W}) dA = \int\int_{\Gamma_F} \bar{\mathbf{t}}_0 \cdot \mathbf{W} dA$$

Finally, the weak formulation consists in finding the vector $\mathbf{u}(\mathbf{X},t)$, implicit in **P** such that

$$\begin{cases} \forall \mathbf{W} \in Adm_1 \text{ find } \mathbf{u}(\mathbf{X},t) \in Adm_2 \text{ that satisfies} \\ \int\int_{\Gamma_F} (\mathbf{t}_0 \cdot \mathbf{W}) dA = -\int\int\int [\rho_0(\mathbf{b} - \mathbf{A}) \cdot \mathbf{W} - \mathbf{P} \cdot \nabla_X \mathbf{W}] dV \end{cases} \tag{13}$$

and the initial conditions (14)

$$\mathbf{x}(\mathbf{X}, t_0) = \mathbf{x}_0(\mathbf{X}) \quad \text{and} \quad \dot{\mathbf{x}}(\mathbf{X}, t_0) = V_0(\mathbf{X}) \tag{15}$$

Let $\phi_i(\mathbf{X}) \in Adm_1$ be a base of a subspace of a Hilbert space. Let the function **u** be expanded in a series of $\phi_i(\mathbf{X})$

$$\mathbf{u}(\mathbf{X},t) \simeq \sum_{i=1}^{N} \boldsymbol{\phi}_i(\mathbf{X}) c_i(t) \tag{16}$$

here $c_i(t)$ are functions only of time.

Replacing the Eq. (16) in (12) we get for each finite element

$$\int\int_{\Gamma_{Fj}} (\mathbf{t}_0(\mathbf{u}) \cdot \boldsymbol{\phi}_j) dA + \int\int\int_{V_j} \left[\rho_0 \left(\mathbf{b} - \sum_{i=1}^{N} \boldsymbol{\phi}_i \ddot{c}_i \right) \cdot \boldsymbol{\phi}_j(\mathbf{X}) - P(u) \cdot \nabla_X \boldsymbol{\phi}_j \right] dV_j = 0 \tag{17}$$

where V_j is the volume of the jth element.

This task was performed with the help of FlexPDE software [14] which is a scripted finite element model builder and a numerical solver.

5. Optimization problem applied to the crack detection

First, the optimization problem is stated. Then, the genetic algorithm is briefly described and the studies carried out to adjust the procedure, are detailed.

5.1. Optimization

The optimization of the inverse problem is attained through a least square criteria, i.e. the dynamic responses obtained from the experimental model are compared with the solution of a computational FEM model at certain points of the structure. The measurements are made at few points (no more than five). The detection problem consists in reconstructing the dynamic with this scarce information in order to solve the inverse problem by introducing the motion data and having the size of the crack as the unknown. In the present study the crack is characterized by two parameters, crack depth (h_c) and location (X_c). Fig. 4 shows an scheme of the dynamic experiment in which a perturbation introduced by hitting a hammer, originates the transverse motion (though any type of motion could be studied). In the Fig. 4, three sensors are shown, *i.e.* accelerometers, at three different locations. Finally, a data acquisitor device completes the setup to obtain the data which yields the time functions $u(X_i, t)$ with $i = 1,\ldots,n$ ($n = 3$ in Fig. 4).

On the other hand, a computational model with crack parameters X_c and h_c of arbitrary values and displacements $u^*(X_i, t)$ at the same points in which the accelerometers were located in the physical experiments, is constructed. The comparison is, then, made between the two functions $u(X_i, t)$ and $u^*(X_i, t)$. The objective function to be optimized in this study is

$$d(X_C, h_C) = \frac{1}{t_2 - t_1} \int_{t_1}^{t2} \sum_{i=1}^{n} [u^*(X_i,t) - u(X_i,t)]^2 dt \tag{18}$$

It was found that this objective function exhibits a large number of local minima. For such a complexity, the usual optimization techniques based on gradient methods are not always successful. Then, an approach based in genetic algorithms is employed to perform the optimization.

5.2. The genetic algorithm (GA) approach

The GA method to solve optimization problems based upon the natural selection is inspired by evolutionary biology. A population of possible solutions of a given problem is generated by this technique. Each of these solutions is named individual. The individuals which are closer to the real solution (i.e. the fitter) will be more capable to pass their (genetic)

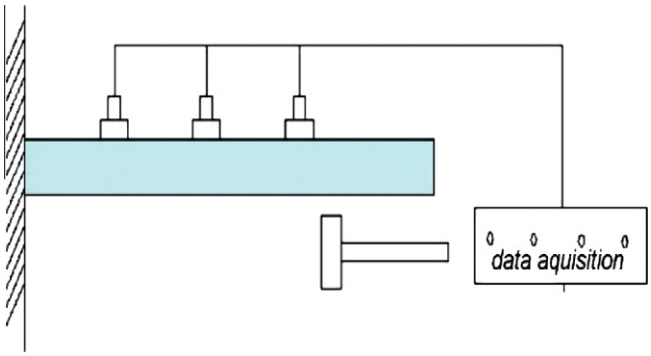

Fig. 4. Scheme of experimental setup to detect the crack in a cantilever beam.

information to the next generation. In each generation the population evolves towards the optimal solution of the problem and the (genetic) information that passes from generation to generation will change according to the following rules:

Selection rule: a selection of the individual named parent is made following certain criterion that contributes to the next generation population.
Crossing rule: two parents are combined to create children for the next generation.
Mutation rule: random changes on the parents individuals are introduced to ensure the (genetic) diversity.

In particular, in the crack detection problem, a set of values $J = (X_{cJ}, h_{cJ})$ is given. Each pair is an individual and the population is the whole set. The GA starts generating a random initial population of individuals. At this stage, it is relevant to guarantee the largest diversity of solutions. Then, new populations are generated. The steps followed in the GA optimization approach are briefly described below. For more detailed information, related bibliography can be consulted e.g. Houck et al. [8], Carneiro [2], Matlab [15].

1. Each individual of the initial population (X_{cJ}, h_{cJ}) is evaluated.
2. The individuals are scaled giving larger scores to the ones that yield a smaller $d(X_{cJ}, h_{cJ})$, i.e. the best fitted.
3. The individuals with larger scores (parents) are selected.
4. New individual are generated (children) through various ways: through random changes of a single parent (mutation), by combining the vector elements of a pair of individuals (crossing) or by identically repeating a child from a parent.
5. The parent population is replaced by the children (new generation).
6. The genetic iteration ends when $d(X_{cJ}, h_{cJ})$ verifies some convergence criterion. Usually two criteria are employed: the GA is run until a maximum number of times is reached or it is stopped when no more changes are evident.

5.3. Adjustment of GA parameters

Different variables were tested to implement the GA algorithm in the crack detection problem by varying one parameter at a time and studying its optimum value. The studied parameters were the simulation time, the number of sensors, the crack depth and location, and more specifically within the GA, the number of individuals, mutation parameters, maximum number of generations, crossing types. In the cracked beam problem, an adjustment study was performed with the following example. A 2D elasticity finite element model is employed to study a clamped-free beam. The length is $L = 2.5$ m, the cross-sectional area is $A = 0.25$ m^2, the modulus of elasticity is $E = 7.3 \times 10^{10}$ Pa, $\nu = 0.3$, and the mass density is $\rho = 2766$ kg/m^3. In this case, the beam is assumed undamped. The dynamics is simulated and the response $u(X_n, t)$ is obtained with $n = 4$ simulating four sensors located at $X_n = nL/5$, that measure the transverse motion of the beam (Fig. 4).

Regarding the GA parameters, the following are considered: uniform initial distribution, rank scaling, stochastic selection, elite count for the reproduction equal to 2 (this means that the two best individuals pass unaltered to the following generation), crossover fraction = 0.8 (*this corresponds to the* 80% *other than elite children*) *and scattered* (*the objective function is only dependent of two variables i.e.* d (X_c, h_c)). The mutation is of the Gaussian type and the stop criteria is a maximum number of ten generations and five repetitions for which the objective function does not improve. Graphics of the fitness function give a clue of the necessary number of generations that are useful in the calculations. Among the parameters, the crossing type was one of the studied. After several runs, it was concluded that the heuristic crossover with $r = 0.6$ was the optimum selection. In order to obtain statistical information of the parameter adjustments, ten scenarios are simulated (Table 1), using the heuristic crossover with $r = 0.6$ and, at this stage, the number of individuals (population) is varied. A maximum number of five generations is adopted. The initial condition is a velocity transverse to the beam axis $V_y = -2X$ and the simulation time is 0.15 s.

The following non-dimensionalized errors are computed

$$e_x = \frac{X_c - X_c^*}{L}; \quad e_h = \frac{h_c - h_c^*}{a}$$

where X_c and h_c are the crack location and depth, respectively, a is the height of the beam cross section, X_c^* and h_c^* are the crack location and depth, respectively, found by GA. The values e_x and e_h are the relative errors of the crack location and depth. The sum $e_r = |e_x| + |e_h|$ is the total error of each simulated scenario, which is a very strong measure. In order to establish the number of individuals necessary to attain acceptable results, the GA is run with different values of populations. The average errors are shown in percentage in Fig. 5. In the studied cases, the GA detects better the damage as the number of individual increases. An average total error less than 10% is considered satisfactory.

Table 1
Simulated scenarios.

Case	1	2	3	4	5	6	7	8	9	10
Crack location X_c	0.1	0.3	0.5	0.7	0.9	1.1	1.3	1.5	1.7	2
Crack depth h_c	0.1	0.1	0.2	0.2	0.1	0.2	0.1	0.2	0.1	0.2

In order to asses the length of the experiment, the GA is run for a population of 50 individuals changing the simulation times. The averaged percentage errors are depicted in Fig. 6. The GA does not improves the detection values as the simulation time increases and the population is kept fixed. The reason is that the objective function $d(X_c, h_c)$ exhibits a larger number of local minima as this variable (simulation time) increases. Consequently, if a detection is desired in the case of a response of large duration, larger populations should be employed. An empirical rule adopted in the present study is to take 50 individuals for the simulation lasting one and a half of the fundamental period of the undamaged specimen.

5.4. Noise influence

Up to this stage, crack detection problems on a beam with a simulated dynamic were dealt with. No uncertainties were included neither in the model nor in the involved parameters. With the aim of studying the robustness of the proposed methodology to more realistic signals, a white noise is now incorporated to the signal of the simulated dynamic, keeping the population (50) and simulation time (0.05 s, approximately one and a half period of the healthy beam). Each of the noise signals has a relative magnitude of 0.1, 0.2 and 0.3 (relative to the tip displacement of the beam). Table 2 depicts the average errors calculated by the sum of two errors ($e_r = |e_x| + |e_h|$) for the same ten scenarios. The robustness of the detection method to this levels of noise can be observed.

5.5. Diffuse crack

The results from the previous subsection encourage the introduction of some type of uncertainty in the problem. A very exact computational model that simulates closely the dynamics of a cracked body is available. But notwithstanding the detailed modeling, it still involves simplifications. A real problem presents uncertainties in the physical model that are

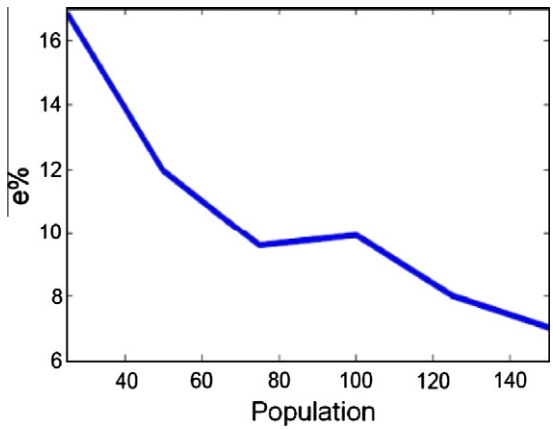

Fig. 5. Influence of the population value.

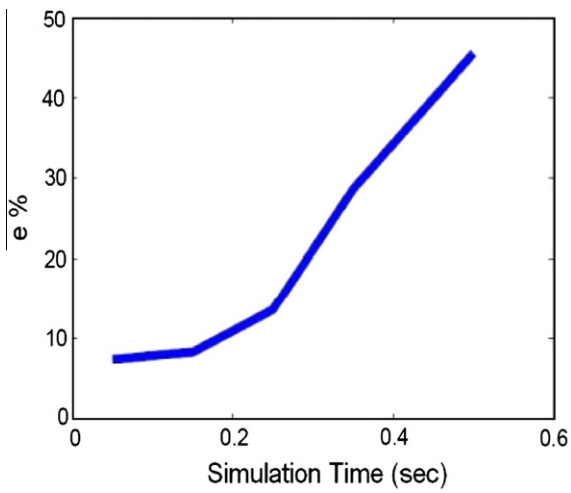

Fig. 6. Influence of the simulation time. Population of 50 individuals.

Table 2
Noise influence. Average errors.

Relative noise	0.1	0.2	0.3
Average error %	6.28	7.71	5.39

approximated with theoretical or computational simulations which will be more or less closer to the physical model. The question that arises is, what happens when a detection is desired in a real specimen with a real crack using this scheme? Let us suppose that the real crack be arbitrary shaped as shown in the left lower part of Fig. 1. Will it be possible to detect such crack if its model is given by the scheme shown in the right lower part of Fig. 1?

To answer this question, the simulation of the cracked beam dynamics is carried out using a crack different from the single crack model. In particular, a "diffuse" type (five cracks in a small region, Fig. 7) is simulated as it were a real experiment of a real body and the model of a single crack used to make the detection. The chosen GA parameters are the individual numbers (50) and the simulation time (0.05 s).

Table 3 contains the six studied cases. The errors are calculated as defined before. Only the 5th. case can be considered a failure.

5.6. Physical experiment

Once the GA parameters and the simulation time have been chosen and accepting certain robustness in the crack shape and the experimental noise, the detection is performed in a real specimen of a clamped beam. Two PASCO accelerometers are employed, each with mass $m = 34.7$ g. The beam is made of aluminum, of length $L = 41.5$ cm (free length), square cross-section of side $a = 0.788$ cm. The accelerometers are located at $X_1 = 23.25$ cm and $X_2 = 34$ cm from the clamped end. Since the model uncertainties are unavoidable, either in the boundary conditions, damping coefficients, elastic modulus or inhomogeneity of the material, a zero setting is carried out to homogenize the parameters in such way that the differences between the computational and physical models be a minimum. Using GA the function,

$$d(E,\mu_d,\mu_{int}) = \frac{1}{t_2 - t_1}\int_{t_1}^{t2}\sum_{i=1}^{2}[u^*(X_i,t) - u(X_i,t)]^2 dt$$

is minimized to find the following parameters: elastic modulus E, the external damping coefficient μ_d (air friction) modeled by the stress vector in the boundary conditions $\mathbf{t} = -\mu_d\mathbf{V}$, and the internal one μ_{int} (linear viscoelastic material) for a period $t_2 - t_1 = 0.1$ s. The GA algorithm was set with a population of 50 individuals, heuristic crossover up to 5 generations, giving the following optimum parameters: $E = 36.567 \times 10^9$ Pa, $\mu_d = 840.57$ Pa s/m. and $\mu_{int} = 7.35$ Pa s.

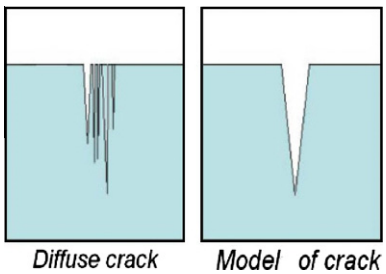

Fig. 7. Diffuse crack models and detection model.

Table 3
Diffuse crack. Six studied cases.

Case (error %)	Case to detect		Detected by GA	
	x_c	h_c	x_c^*	h_c^*
1 (7.16)	0.3	0.1	0.32	0.115
2 (8.12)	0.7	0.1	0.55	0.105
3 (4.64)	1.3	0.2	1.25	0.206
4 (6.72)	1.5	0.2	1.36	0.197
5 (41.3)	1.9	0.1	2.37	0.044
6 (6.51)	1	0.12	0.98	0.134

In order to reproduce the same initial condition in the physical test, a weight of mass $m = 266.12$ g is hung from the free end of the beam. Then, to initiate the motion, the thread is cut with fire. Thus, a minimum perturbation in the initial condition is ensured. The two motion sensors register the vibration motion of the undamaged beam in the acquisitor. Fig. 8a shows the accelerations at points X_1 and X_2 for the experiment and Fig. 8b, the ones corresponding to the simulation with the optimal parameters, taking into account the masses and location of the accelerometers.

Certain similarity is observed in the acceleration amplitudes as well as the dissipation of the signals.

To assess the damage in the beam and once the model is calibrated, notches are made with different depths: 2.6 mm ($h_c/a = 0.329$), 4 mm ($h_c/a = 0.507$) and 5 mm ($h_c/a = 0.634$) and of 1 mm width, at 14 cm ($X_c/L = 0.337$) from the fixed end (see Fig. 9).

Again, the optimization of $d(X_c, h_c)$ is made for the time $t_2 - t_1 = 0.1$ s using $E = 36.567 \times 10^9$ Pa, $\mu_d = 840.57$ Pa s/m and $\mu_{int} = 7.35$ Pa s with GA parameters: a population of 75 individuals and heuristic crossover with up to 5 generations.

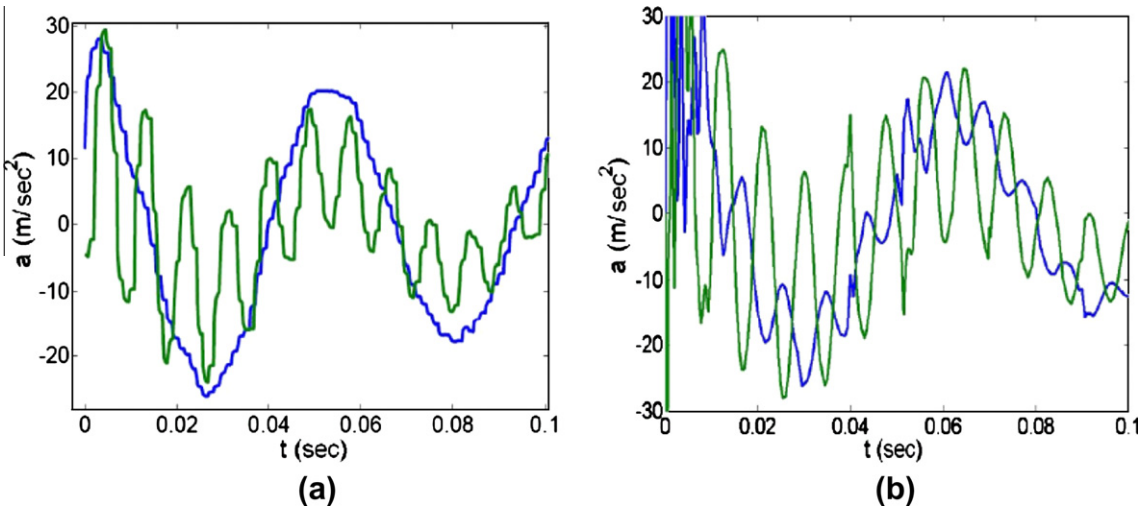

Fig. 8. (a) Acceleration at points x_1 (blue) and x_2 (green) for the undamaged beam. Physical model. (b) Acceleration at points x_1 (blue) and x_2 (green) for the undamaged beam. Computational model. (For interpretation of the references to colour in this figure legend, the reader is referred to the web version of this article.)

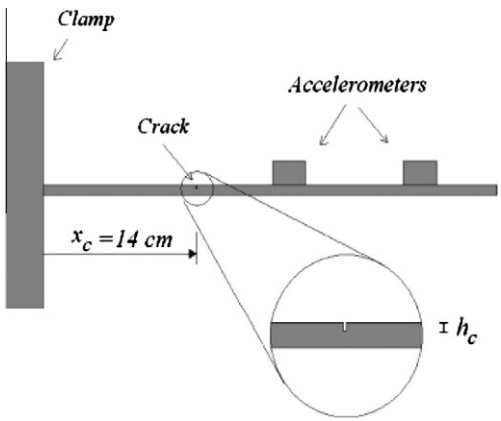

Fig. 9. Scheme of the cracked aluminum beam.

Table 4
Crack parameters detected with GA using a physical experiment.

Case	x_c/L	h_c/a	x_c/L detected	h_c/a detected	Error %
1	0.337	0.329	0.378	0.257	11.2
2	0.337	0.507	0.282	0.366	19.6
3	0.337	0.634	0.357	0.548	10.6

The detection results for each of the three damage scenarios are detailed in the Table 4. As can be seen, the values of position and depth of damage are determined with good accuracy. This shows that the methodology could be employed to detect crack depth and position considering the opening and closure of the crack in a dynamic experiment of a damaged specimen. At this stage of the study, the experiment was performed which rather low precision instrumental in order to design the methodology. Nevertheless, the results can be considered encouraging.

5.7. Detection in an arch

Now, a curved structural element is studied. In principle, any two or three dimensional shape may be used. In this case, a circular arch, as showed schematically in Fig. 10, is proposed. The arch is fixed at both ends (null displacement) and free at the rest of this contour, *i.e.* zero stress ($\mathbf{t} = 0$) across the border except in the region of the crack where, as before, Signorini contact conditions are imposed.

The interesting thing about this geometry is that there is no symmetry between top and bottom. Nevertheless, the problem is able to detect whether the crack is on the top or on the bottom of the beam. The idea is very simple. The position of the crack will have a value going from 0 to L and from L to $L^{'}$ that is, doubling the domain of definition of the variable X_c in the objective function.

In particular, we study a circumferential arch of 180° opening angle with an inner radius of 6 m and an outer radius of 9 m. Then, the length ranging from 0 to L (outer radius) is parametrized from 0 to 9π, and for the inner radius, 9π to $(9+6)\pi$. In short, $X_c \in (0, 15\pi\text{m}) \simeq (0, 47.12\text{ m})$. A 2D model is assumed. In this case, the material is modeled by an elastic modulus $E = 7 \times 10^9$ Pa with a density $\rho_0 = 2000$ kg/m^3. To construct the objective function, a time window $\Delta t = 0.035$ s was employed. This interval corresponds approximately to 1.5 periods of the fundamental frequency for the non-cracked arch in the linear case. Six crack scenarios were addressed.

Table 5 depicts the different scenarios and the detected parameters. The population parameters of the GA method are the same as above. The resulting errors for the detection of cracks in the arch are of similar magnitude to those found in the beam case.

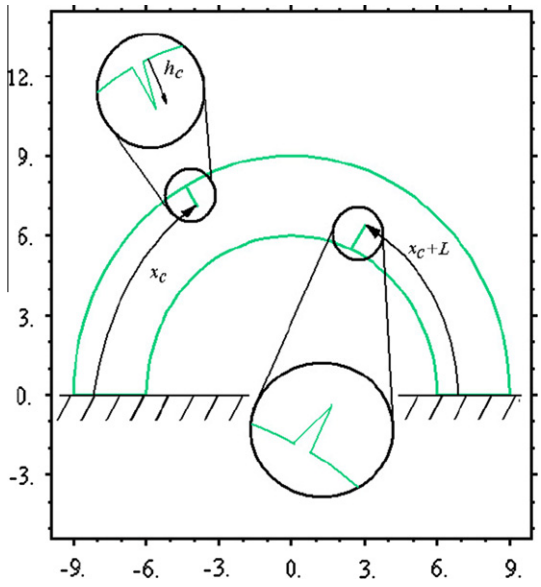

Fig. 10. Scheme of the cracked arch.

Table 5
Results and errors for the detection of damage in the arch.

Case (error %)	Case to detect		Detected by GA	
	x_c	h_c	x_c^*	h_c^*
1 (6.864)	10	0.1	12.91	0.0798
2 (36.81)	10	1	15.55	1.75
3 (9.152)	23	1.2	25.52	1.314
4 (4.576)	35.5	2	34.93	2.101
5 (9.032)	39	1	41.13	1.135
6 (9.198)	45	0.12	41.02	0.0981

5.8. Crack detection in a blade-like element

Since the developed computational model is general with respect to the type of motion (large deformations, rotations and displacements) and the geometry, 3D models of arbitrary shaped structural elements can be studied. As was mentioned in the Introduction section, the advantage of a general model is not only restricted to account for finite strains but also to finite rotational motion. Figs. 11 and 12 depict a scheme of a blade-like element that could resemble for instance, the blade of a wind turbine. The blade geometry is generated by a plane that models the plane shape with a length $L = 8$ m and a maximum width of $a = 1.55$ m. The blade is very thin (0.08 m) and the warping along its length is given by $Z(X, Y) =$

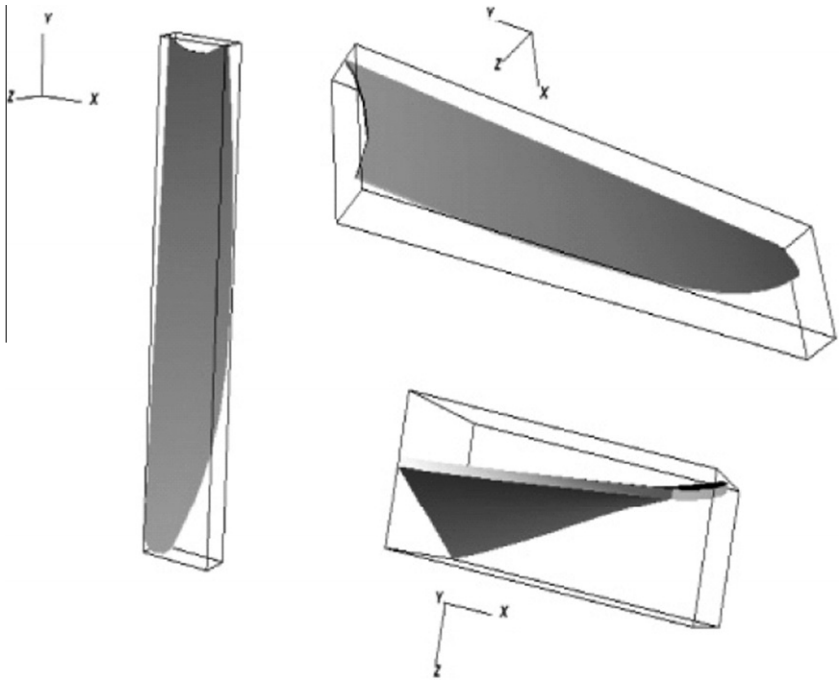

Fig. 11. Views of the 3D blade-like structural element.

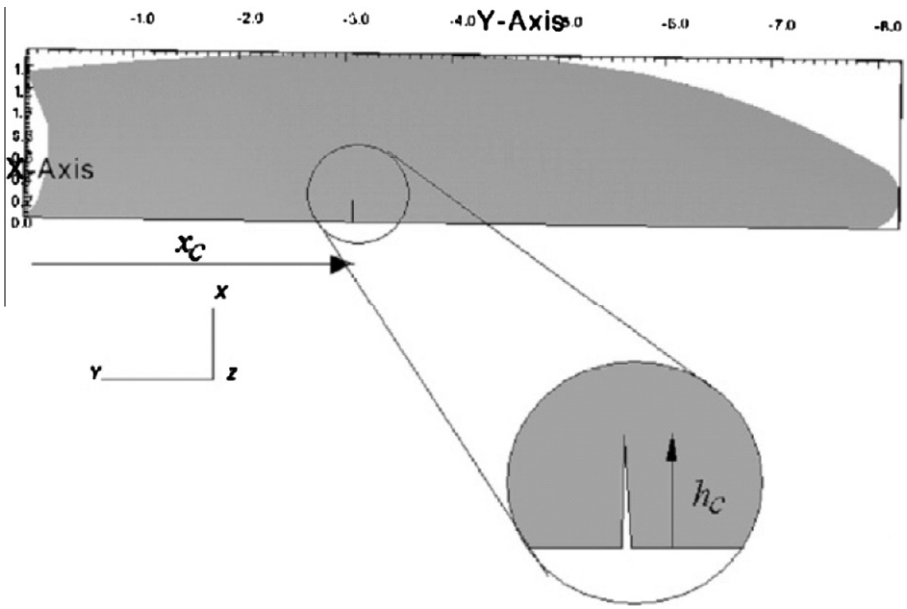

Fig. 12. Cracked blade.

Table 6
Simulated scenarios in a 3D blade-like element.

Case	$x_c\,(m)$	$h_c\,(m)$
1	3	1
2	2.3	0.1
3	2.3	0.15
4	4.3	0.15
5	7.3	0.05

Table 7
Crack detection in a 3D blade-like element.

Case	x_c/L	h_c/a	x_c/L detected	h_c/a detected	Error %
1	0.375	0.64516	0.3539	0.67806	5.4
2	0.2875	0.064516	0.31270	0.05805	3.166
3	0.2875	0.096774	0.29451	0.08857	1.521
4	0.5375	0.096774	0.767432	0.19112	32.42
5	0.9125	0.032258	0.885763	0.03363	2.811

$\pm\, 0.02 + 0.04{\cdot}Y{\cdot}(X-1) - 0.1{\cdot}X$. The blade rotates at 10 rad/s around axis z and a simulation of almost a complete rotation is done during 0.5 s without including noise. The material is steel and its constitutive law is given by Eq. (6) where the Lamé constants correspond to steel and are found with $E = 2.05 \times 10^{11}$ Pa and $\nu = 0.3$. The GA parameters are: population 75, 10 generations, heuristic crossover with $r = 0.6$. Crack scenarios are detailed in Table 6, being the GA parameters kept constant. The resulting errors for the detection of cracks in the blade-like element are in the same range as before. The results are shown in Table 7.

6. Detection using static measures

Frequently, it is not difficult in practise to obtain accurate static displacement measurements through gauges at some points of the body. Alternatively, optic interferometry techniques can provide of such data.

For the cases in which the displacements can be measured in a reduced set of points, this information can by used to detect damage.

Let us analyze a body in equilibrium. If the deformation is finite, it will satisfy the equilibrium equation

$$\nabla \cdot (\mathbf{FS}) + \rho_0 \mathbf{b} = \mathbf{0}$$

where $\mathbf{S} = g'(\mathbf{E})$ is the second Piola–Kirchhoff stress tensor given by a constitutive relationship (Eq. (6))

The Signorini contact model (10) and its regularization (11) are applied similarly to the dynamic case. Obviously, the static case is the particular case of dynamic one.

In order to systematize the development of the GA, we will proceed to study a fixed-free beam of the same size as before in the example of Section 5.3, that is: length $L = 2.5$ m cross-sectional area is $A = 0.25$ m^2, and elastic material with a modulus of elasticity $E = 7.3 \times 10^{10}$ Pa, Poisson ratio $\nu = 0.3$ density $\rho_0 = 2766$ kg m^{-3}.

Suppose that we have a quantity n of sensors measuring the transverse displacement arranged along the beam, equidistant one to the other as is shown in Fig. 4. This beam is deformed by the application of some action, for example a known force, and the sensors measure the deformation.

Scenarios given in Table 1 are simulated in this case and a load of 7840 kN is applied twice in the transverse direction (upward and downward). Fig. 13 depicts the upward case. This is because the crack could be on one side or on the other. This will automatically give twice as much data to analyze.

The objective function is then

$$d(X_C, h_C) = \sum_{i=1}^{n} \left[u^{\uparrow *}(x_i) - u^{\uparrow}(x_i)\right]^2 + \sum_{i=1}^{n} \left[u^{\downarrow *}(x_i) - u^{\downarrow}(x_i)\right]^2 \tag{19}$$

The symbols $\uparrow$ and $\downarrow$ in (19) indicate when the load is upward or downward, respectively.

As is done in the dynamic case, the model is calculated for the case of an arbitrary crack, *i.e.* a position and depth (X_C and h_C) and the displacements are obtained at the same points x_i that were used at the simulated experiment $u^*(x_i)$ with $i = 1, \ldots, n$ (n number of sensors). Fig. 13 shows the deformation in the event that the load is applied upward. In Fig. 13a) it is apparent that 7840 kN are not sufficient to close the whole crack, though this value is enough to obtain a measurable deformation. Fig. 13b) shows the stresses at the crack faces where contact occurs.

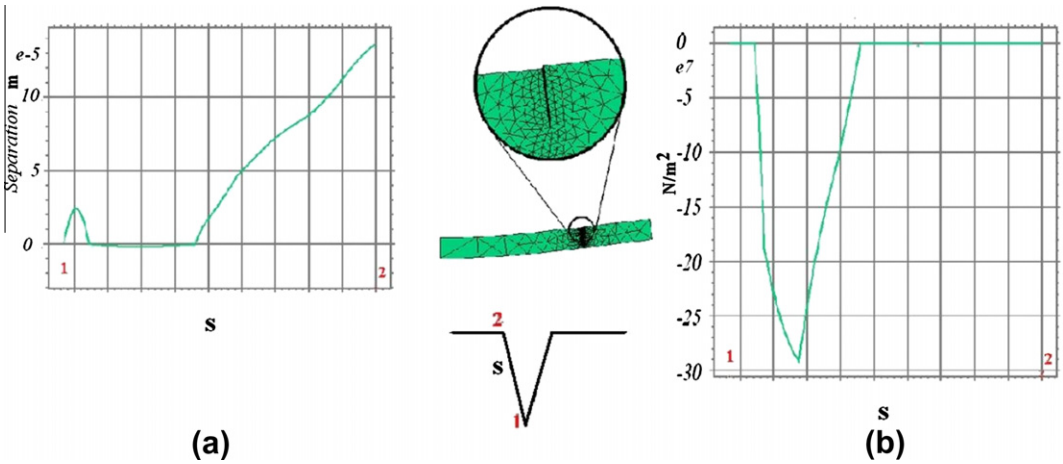

Fig. 13. Damaged beam. Static case (a) Distance between the two sides of the fracture. (b) Contact stress in the fracture. The variable s indicates the length of the segment that goes from 1 to 2 on the crack interface.

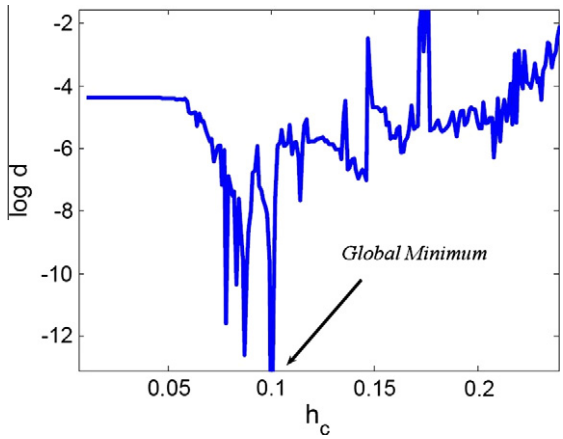

Fig. 14. Function log (d) showing large number of local minima.

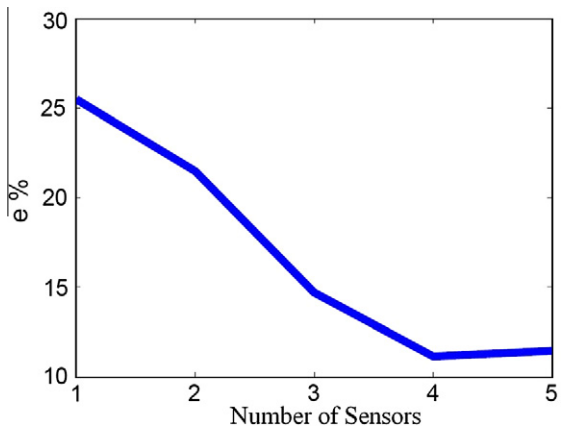

Fig. 15. Detection error as a function on the number of sensors.

As before, the objective function presents many local minima. Fig. 14 is a graphical representation on a log scale of the function d by setting the value of X_C (crack location) and varying the depth value h_C. A large number of local minima can be observed.

Fig. 15 shows how the average error decreases in the 10 cases reported in Table 1 as the number of sensors in the experiment increases. Four sensors appear to be sufficient for the crack detection in a straight bar. Recall that 10% error is more

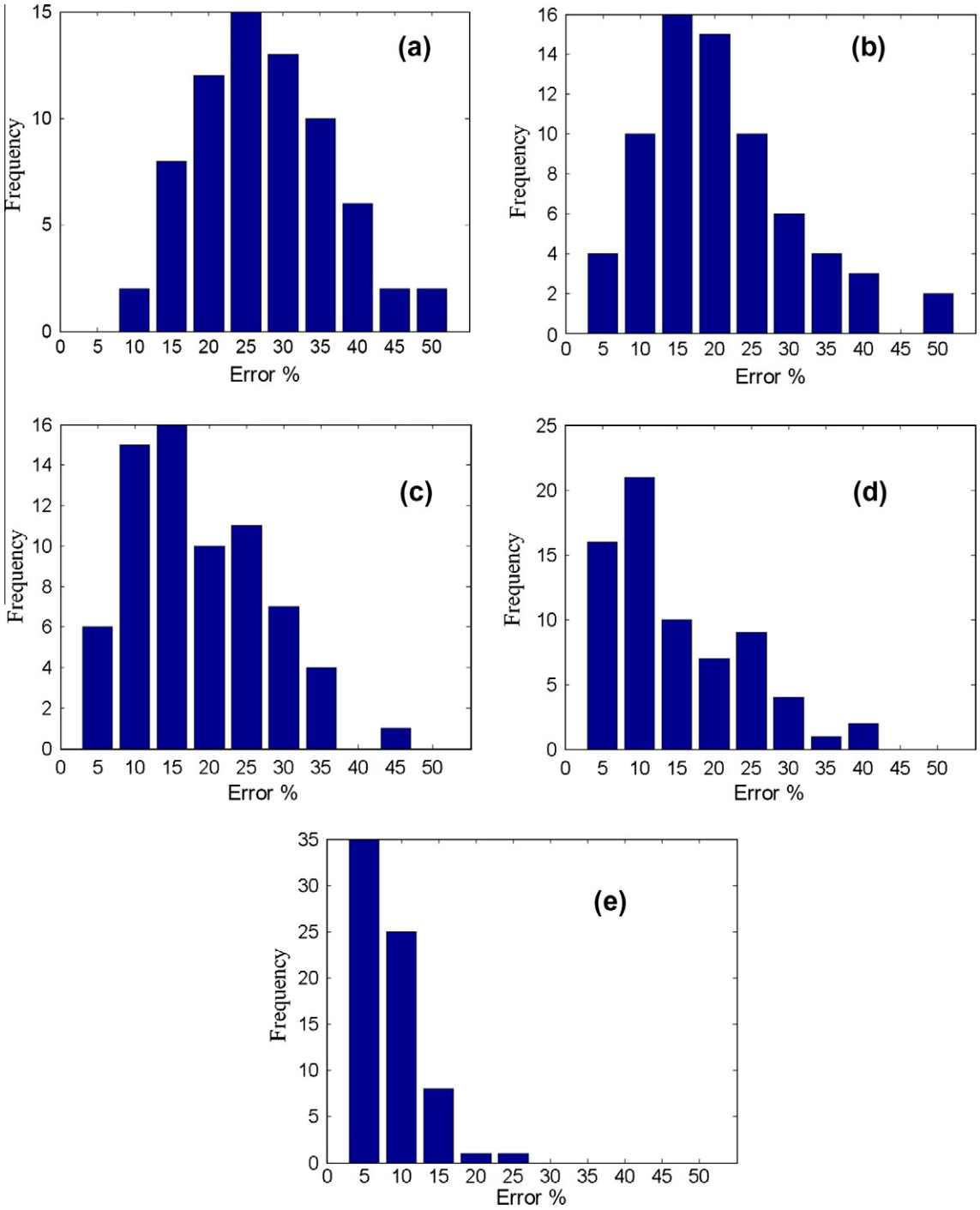

Fig. 16. (a) Distribution of percentage errors for a population of 40 individuals in the GA method. (b) Idem (a) of 60 individuals in the GA method. (c) Idem (a) of 80 individuals in the GA method. (d) Idem (a) of 100 individuals in the GA method. (e) Idem (a) of 120 individuals in the GA method.

than satisfactory since the convention used for its calculation is the sum of the errors to find the two parameters, namely crack position and depth.

6.1. Statistical distributions in the detection

An extense statistical study is performed in order to illustrate the distributions of the detection error in the case of static measures as the number of individuals in the AG changes. That is, it seeks to study the efficiency of evolutionary algorithms as a function of populations.

The study consists of 70 different damage scenarios randomly generated for the beam of Fig. 13. The detection of the damage is made using the objective function defined by Eq. (19) where displacements are measured at four points (*i.e.* $n = 4$), in $X_n = nL/5$. This numerical experiment is performed five times for populations of 40, 60, 80, 100, and 120 individuals, respectively. All other GA parameters are unchanged. It should be noted that this numerical-computational study involves the calculation of $70 \times 5 = 350$ different scenarios. Fig. 16a corresponds to the case of 40 individuals. In this Figure, a symmetrical distribution of the errors around the center is observed. In this case the average corresponds to 27.5% error. Fig. 16b corresponds to the case of a population of 60 individuals. In this case, we can see how the errors are distributed skewed to the left of the maximum value. The average error corresponds to 20.7%. Fig. 16c corresponds to the case of a population of 80 individuals. Now, we can see more clearly how the errors are shifted to the left of the maximum value. In this case, the average corresponds to 18.7% error. The distribution of errors for 100 individuals is plotted in Fig. 16d. There, the maximum frequency of errors is between 5% and 10% although the average is 14.5% . Finally, the distribution for the case of 120 individuals is plotted in Fig. 16e. In this case, the dispersion is a minimum with a maximum between 0% and 5% and an average error of 8.1%.

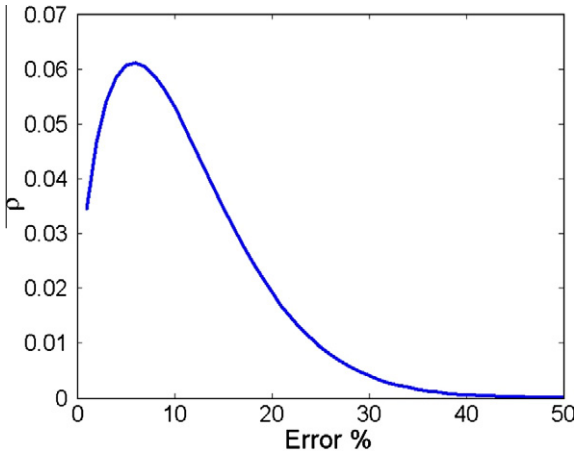

Fig. 17. Weibull distribution for the detection error with a population of 60 individuals.

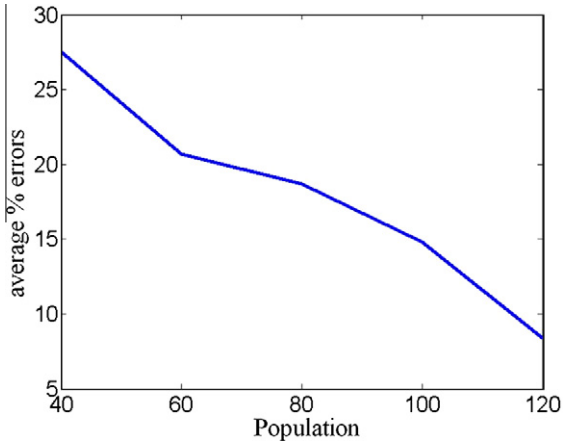

Fig. 18. Average error in the detection of damage via static tests as a function of the number of individuals in the population of AG method.

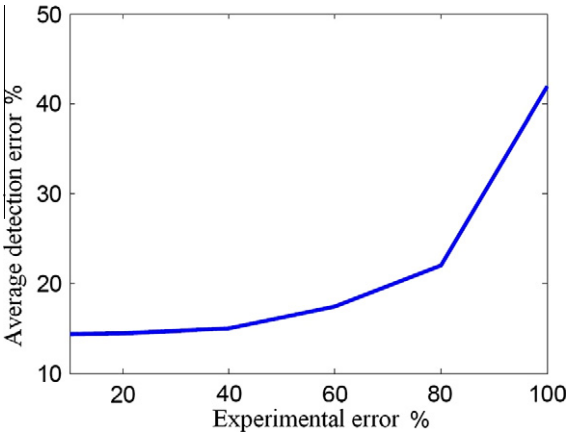

Fig. 19. Average detection error as a function of experimental error.

Given that the error cannot attain negative values, empirically, one can assume that the distribution of errors in detection via GA is of the Weibull type. This distribution is defined by

$$\rho(x) = abx^{b-1}e^{-ax^b} \tag{20}$$

where a and b are two parameters that characterize the distribution defined by the variance σ^* and the average μ^*

$$\mu^* = a^{-1/b}\Gamma(1+b)$$
$$\sigma^{*2} = a^{-2/b}\left[\Gamma(1+2/b) - \Gamma^2(1+1/b)\right]$$

It was found that a value of $b = 1.45$ gives a reasonable description for all cases.

Weibull distribution for the detection error with a population of 60 individuals is depicted in Fig. 17, *i.e.* it is comparable with Fig. 16b). Finally, the average percentage errors of these numerical experiments for the detection via static measurements are showed in Fig. 18. We can see that, as the number of individuals in the population is increased, the error decreases. Comparing this result with that of Fig. 5, it can be concluded that the damage detection via dynamic experiments is more accurate, as could be expected. It is the richness of information in the dynamic measurement which gives the possibility of a solution of the inverse problem more accurate than in the static case.

6.2. Influence of experimental error in the static measurement

Since in a real test, measurement errors are unavoidable, and the last object of these studies is the experimental implementation, we added an uncertainty, a random number r to the simulated experiment results. That is, data were taken as the value $u(X_i) + r$ and the minimum of Eq. (19) was found via GA.

Fig. 19 shows the average error in the same 70 damage scenarios randomly generated as the measurement error is increased. Here, the simulated experimental error is taken as the percentage referred to the displacement of the tip of the bar (the maximum). It can be seen that it is possible to detect damage when the experimental information involves an error up to 40% in the deformation using only four sensors ($n = 4$) in a single experiment.

In general, the dynamic method gives more accurate results but it is computationally more expensive than the static one.

It is interesting to observe how a technique based on searching parameters by GA is successful even in complex situations with large experimental errors and uncertainties between the computer model and physical model.

7. Final comments

A methodology based on genetic algorithms for the crack detection on damaged structural elements was presented. The technique proved to be successful in the studied cases and allows up to level-three detection. The optimization is applied to an objective function constructed from the dynamics of the studied body. This dynamics is modeled within Continuum Mechanics with a Lagrangian reference which yields advantages when a contact model at the crack interfaces is desired. The breathing crack was idealized either by a straight notch or a wedge and following Signorini contact theory of two bodies with finite deformations. Since arbitrary shaped bodies can be handled with the present nonlinear elasticity approach, different shapes crack, realistic contact simulations, arbitrary motions and arbitrary shaped structural elements, can be tackled. First, crack detection was performed using computational experiments and afterwards a physical experiment on a beam was employed to validate the methodology. Extensive computational studies were performed to calibrate and find the optimum

GA parameter values and the damaged body dynamics. One conclusion drawn from the studied cases, is that the number of individuals should be proportional to the simulation time (for long time periods). Additionally, the crack detection was applied in an arch with a 2D model and in a blade-like structural element, through a 3D model while in operational regime. This last element could be the representation of a wind turbine blade, undergoing rotation. The nonlinear elasticity frame together with the FEM implementation allows to extend the methodology to any arbitrary shaped body for any type of motion (for example finite rotations).

In the use of GA, the computational dynamic model is solved a number of times equal to the number of individuals in the population multiplied by the number of generations. For example, if 75 individuals and a maximum of 10 generations are chosen, the search pattern should be resolved 750 times. One could argue that the latter would require a large computational cost. However, since each case is unrelated one to the other, the search technique based on GA can be easily implemented in distributed computing. Indeed, there is a trend in recent years to multi-processor computers. This justifies to implement search techniques using complex models because the computational cost will decrease.

References

[1] Carlin RA, Garcia E. Parameter optimization of a genetic algorithm for structural damage detection. In: International modal analysis conference, vol. 18; 1996. p. 194–200.
[2] Carneiro SHS. Model-based vibration diagnostic of cracked beams in the time domain. PhD thesis, Faculty of the Virginia Polytechnic Institute and State University; 2000.
[3] Carneiro SHS, Inman DJ. Continuous model for the transverse vibration of cracked Timoshenko beams. ASME J Vib Acoust 2002;124:310–20.
[4] Carneiro SHS, Inman DJ. Comments on the free vibrations of beams with a single-edge crack. J Sound Vib 2001;244(4):729–36.
[5] Dimarogonas AD. Vibration of cracked structures: state of the art review. Engng Fract Mech 1996;55:831–57.
[6] Doebling SW, Farrar CR, Prime MB. A summary review of vibration-based damage identification methods. Shock Vib Dig 1998;32:2.
[7] Eringen AC. Mechanics of Continua, vol. I. Robert E. Krieger Publ. Co.; 1980.
[8] Houck CR, Joines JA, Kay MG. A genetic algorithm for function optimization: a Matlab implementation. In: Tech Rep NCSU-IE, 95:09;1995.
[9] Johnson KL. Contact mechanics, vol. I. Cambridge University Press; 1987.
[10] Khiema NT, Lienb TV. Multi-crack detection for beam by the natural frequencies. J Sound Vib 2004;273:175–84.
[11] Kikuchi N and Oden JT. Contact problems in elasticity a study of variational inequalities and finite element methods. In: Studies in applied mathematics;1998.
[12] Kim JT, Stubbs N. Crack detection in beam-type structures using frequency data. J Sound Vib 2003;259:145–60.
[13] Lai WM, Rubin D, Krempl E. Introduction to continuum mechanics, vol. I. Butterworth-Heinemann Ltd.; 1993.
[14] Law SS, Lu ZR. Crack identification in beam from dynamic responses. J Sound Vib 2005;285:967–87.
[15] Matlab. Genetic algorithm and direct search toolbox 2.3. V.7; 2006.
[16] Owolabi ASJ, Swamidas G, Seshadri R. Crack detection in beams using changes in frequencies and amplitudes of frequency response functions. J Sound Vib 2003;265:1–22.
[17] Rao BN, Rahman S. A continuum shape sensitivity method for fracture analysis of isotropic functionally graded materials. Comput Mech 2006;38:133–50.
[18] Raous M. Quasistatic Signorini problem with coulomb friction and coupling to adhesion. In: New developments in contact problems. CISM courses and lectures, vol. 384; 1999[chapter 3].
[19] Rosales MB, Filipich CP, Buezas FS. Crack detection in beam-like structure. Engng Struct 2009;31:2257–64.
[20] Salawu OS. Detection of structural damage through changes in frequency: a review. Engng Struct 1997;19:718–23.
[21] Truesdell C, Noll W. The non-linear field theories of mechanics, vol. I. Berlin, Heidelberg (New York): Springer-Verlag; 2003. p. 1037–47.
[22] Wang BS, He ZC. Crack detection of arch dam using statistical neural network based on the reductions of natural frequencies. J Sound Vib 2007;302:1037–47.